

# Planetary-Scale Wave Structures of the Earth's Atmosphere Revealed from the COSMIC Observations

S. K. A. V. Prasad Rao ANISETTY<sup>1</sup>, P. S. BRAHMANANDAM<sup>2\*</sup>, G. UMA<sup>3</sup>, A. Narendra BABU<sup>4</sup>, HUANG Ching-Yuang<sup>1</sup> (黄清勇), G. Anil KUMAR<sup>5</sup>, S. Tulasi RAM<sup>6</sup>, WANG Hsiao-Lan<sup>1</sup> (王筱岚), and CHU Yen-Hsyang<sup>2</sup> (朱延祥)

<sup>1</sup> Department of Atmospheric Sciences, National Central University, Chung-Li 32001, Taiwan, China

<sup>2</sup> Institute of Space Science, National Central University, Chung-Li 32001, Taiwan, China

<sup>3</sup> Department of Electronics and Communication Engineering, Koneru Lakshmaiah University, Vaddeswaram 522540, India

<sup>4</sup> Department of Electronics and Communication Engineering, Lakkireddy Bali Reddy Engineering College, Mylavaram 521230, India

<sup>5</sup> Department of Physics, K L University, Vaddeswaram 522540, India

<sup>6</sup> Indian Institute of Geomagnetism, New Panvel, Navi Mumbai 410218, India

(Received July 31, 2013; in final form October 22, 2013)

## ABSTRACT

GPS radio occultation (GPS RO) method, an active satellite-to-satellite remote sensing technique, is capable of producing accurate, all-weather, round the clock, global refractive index, density, pressure, and temperature profiles of the troposphere and stratosphere. This study presents planetary-scale equatorially trapped Kelvin waves in temperature profiles retrieved using COSMIC (Constellation Observing System for Meteorology, Ionosphere, and Climate) satellites during 2006–2009 and their interactions with background atmospheric conditions. It is found that the Kelvin waves are not only associated with wave periods of higher than 10 days (slow Kelvin waves) with higher zonal wave numbers (either 1 or 2), but also possessing downward phase progression, giving evidence that the source regions of them are located at lower altitudes. A thorough verification of outgoing longwave radiation (OLR) reveals that deep convection activity has developed regularly over the Indonesian region, suggesting that the Kelvin waves are driven by the convective activity. The derived Kelvin waves show enhanced (diminished) tendencies during westward (eastward) phase of the quasi-biennial oscillation (QBO) in zonal winds, implying a mutual relation between both of them. The El Niño and Southern Oscillation (ENSO) below 18 km and the QBO features between 18 and 27 km in temperature profiles are observed during May 2006–May 2010 with the help of an adaptive data analysis technique known as Hilbert Huang Transform (HHT). Further, temperature anomalies computed using COSMIC retrieved temperatures are critically evaluated during different phases of ENSO, which has revealed interesting results and are discussed in light of available literature.

**Key words:** radio occultation technique, Kelvin waves, outgoing long-wave radiation (OLR), quasi-biennial oscillation (QBO), El Niño and Southern Oscillation (ENSO)

**Citation:** Anisetty, P. Rao, P. S. Brahmanandam, G. Uma, et al., 2014: Planetary-scale wave structures of the earth's atmosphere revealed from the COSMIC observations. *J. Meteor. Res.*, **28**(2), 281–295, doi: 10.1007/s13351-014-0101-y.

## 1. Introduction

It is generally known that the equatorial region receives relatively higher solar radiation compared to po-

lar regions; consequently, the equatorial region acts as a source for various atmospheric wave modes. Among these, Kelvin waves or Rossby-gravity waves are most important equatorial wave modes that are forced in

Supported by the Science Council of Taiwan (NSC-101-2811-M-008-012).

\*Corresponding author: anandp@jupiter.ss.ncu.edu.tw.

©The Chinese Meteorological Society and Springer-Verlag Berlin Heidelberg 2014

the tropical troposphere by convective processes (Pires et al., 1997; Lindzen, 2003; Randel and Wu, 2005; Brahmanandam et al., 2010). The planetary-scale (wavenumber  $n = 1$  or  $2$ ) eastward propagating equatorially trapped Kelvin waves often show periods ranging from a few days to a few tens of days. It is true that considerable progress has been achieved in studying the Kelvin waves ever since their discoveries by Wallace and Gousky (1968), who used radiosonde measurements including winds and temperatures to characterize the Kelvin waves.

In addition to radiosonde instruments (Wallace and Gousky, 1968; Tsuda et al., 1994; Fujiwara et al., 2001; Sridharan et al., 2006), Mesosphere Stratosphere Troposphere (MST) radars (Sasi and Deepa, 2001) have been used to observe Kelvin waves before the era of satellite remote sensing techniques. Though radiosondes and MST radars can provide data with excellent vertical resolution, due to their meager presence at equatorial regions, they are of no use to study the global characteristics, particularly horizontal propagation characteristics, of these equatorial planetary-scale waves. Later, limb viewing satellite remote sensing instruments including LIMS, MLS, CLEAS, and CRISTA have contributed enormously to understanding of the Kelvin wave modes in stratospheric altitudes (Salby et al., 1984; Canziani et al., 1994; Shiotani et al., 1997; Smith et al., 2002) through revealing of Kelvin wave variability that lies in the zonal wavenumber range of 2–3. Nevertheless, these limb viewing satellites have their own shortcomings in evaluating Kelvin waves of the short to very short period and vertical wavelength, due to their poor temporal resolution.

It has been well recognized that Kelvin waves can significantly influence the tropopause structure (Tsuda et al., 1994; Randel and Wu, 2005; Ratnam et al., 2006), thereby play an important role in the stratosphere-troposphere exchange of ozone (Fujiwara et al., 1998), dehydrating air entering the lower stratosphere from the upper troposphere (Fujiwara et al., 2001), and occurrence of convective turbulence near the tropopause (Fujiwara et al., 2003). Most importantly, large-scale Kelvin and Rossby-gravity waves

are thought to play an important role in driving the eastward phase of quasi-biennial oscillation (QBO) of the zonal winds of the equatorial stratosphere (Angell and Korshover, 1964; Holton and Lindzen, 1972). Observational and numerical modeling studies suggest that the momentum fluxes of Kelvin and Rossby-gravity waves are too meager (by factors of 2–4) to drive QBO, and gravity waves probably play an important role (Hitchman and Leovy, 1988; Alexander and Holton, 1997; Dunkerton, 1997; Canziani and Holton, 1998; Baldwin et al., 2001; Kawatani et al., 2010; Evan et al., 2012). Some studies (Tindall et al., 2006a, b; Alexander et al., 2008; Ern et al., 2008) have speculated that higher wavenumber (4–7) eastward and westward propagating equatorially trapped waves along with gravity waves contribute significantly to the total momentum flux transfer, which in turn plays a key role in the dynamics of the QBO.

Contrary to above, it has been reported that the phase of ENSO will have substantial impacts on Kelvin waves and associated convection over the equatorial central-eastern Pacific in such a way that El Niño (La Niña) events enhance (suppress) the variability of upper tropospheric Kelvin wave and the associated convection there (Yang and Hoskins, 2013). It was postulated by Yang and Hoskins (2013) that the mechanism of the impact is through changes in the ENSO related thermal conditions and the ambient flow. In El Niño years, because of SST increase in the equatorial central eastern Pacific, variability of the eastward-moving convection, which is mainly associated with Kelvin waves, intensifies in the region. In addition, due to weakening of the equatorial eastern Pacific westerly duct in the upper troposphere in El Niño years, Kelvin waves amplify there.

On the other hand, the issues such as poor spatial and temporal resolutions can be resolved if one uses the database provided by global positioning system (GPS) radio occultation (RO) technique. The main advantages of GPS RO products are their unprecedented vertical resolution, global coverage, all weather capability, and high accuracy. Though the earth's atmosphere has been monitored with RO techniques including mono-satellite GPS/MET (Melbourne et al.,

1994), CHALLENGING Mini satellite Payload (CHAMP; Wickert et al., 2001), and Satellite de Aplicaciones Cientificas-C (SAC-C; Hajj et al., 2004), due to their relatively sparse sampling, only seasonal or multiyear phenomena of equatorial waves could be studied. As a boon to the scientific community, the launch of six COSMIC (Constellation Observing System for Meteorology, Ionosphere, and Climate) satellites provides an order of magnitude increase in the number of GPS-RO profiles available (Anthes et al., 2008). It has been estimated that COSMIC satellites provide approximately 12 times higher amount of data than the earlier RO missions, and on average about 1500–2000 profiles are available during a day around the globe (Brahmanandam et al., 2010; Anthes, 2011). It is, therefore, expected that the COSMIC constellation will provide much more detailed analysis of wave structures with higher wave numbers in the lower atmosphere (Alexander et al., 2008; Brahmanandam et al., 2010). Note that the COSMIC GPS RO technique has already provided significant research results in ionospheric altitudes (Brahmanandam et al., 2011; Chu et al., 2011; Potula et al., 2011; Brahmanandam et al., 2012; Uma et al., 2012).

Due to high vertical resolution and global coverage of the RO data provided by COSMIC satellites, several research attempts have been made to describe the global characteristics of gravity, Rossby-gravity, and Kelvin waves, and their three-dimensional large-scale structures in the troposphere and lower stratosphere. For example, Alexander et al. (2008) by effectively utilizing temperature profiles retrieved from COSMIC satellites have studied equatorial gravity waves, equatorially trapped Kelvin waves, and mixed Rossby-gravity waves with zonal numbers  $\leq 9$ , and their interaction with the background QBO wind. The study conducted by Scherllin-Pirscher et al. (2012) on the vertical and spatial structure of the atmospheric ENSO using COSMIC RO retrieved temperature data has revealed that during warm phase of ENSO, the zonal-mean temperatures increase in the tropical troposphere and decrease in the tropical stratosphere. Zeng et al. (2012) used both temperature and specific humidity profiles derived from 4-

yr COSMIC RO measurements to study the vertical structure of the Madden-Julian Oscillation (MJO). In the present study, we focus exclusively on Kelvin wave characteristics, i.e., how Kelvin waves respond to different phases of QBO, and the relation of temperature anomalies to different phases of ENSO during 2006–2010. In this context, some important observational results are noticed, which will be discussed in light of available literature in the ensuing sections.

In addition to the COSMIC retrieved temperature profiles, we have also used radiosonde measured zonal winds over Singapore ( $1^\circ\text{N}$ ,  $104^\circ\text{E}$ ), an equatorial station, to assess the background atmospheric dynamics. Further, daily gridded outgoing long-wave radiation (OLR) data provided by the NOAA Climate Diagnostics Center are used as a proxy for tropical convection in the present study.

The organization of this article is as follows. In Section 2, we present brief descriptions of the RO technique employed by COSMIC satellites, the ENSO phenomenon, and the famous HHT method. In Section 3.1, we present basic comparisons of vertical temperature profiles from radiosonde and from the COSMIC RO technique. In Section 3.2, we present characteristics of the planetary-scale waves observed by using the COSMIC retrieved temperature profiles. Section 3.3 provides observed ENSO and QBO features in the COSMIC temperature profiles. Finally, conclusions are given in Section 4.

## 2. Concepts and methodology

### 2.1 About the GPS RO technique

Though scientists have long recognized the usefulness of radio occultation in studies of the planetary atmosphere as early as in 1971 (Fjeldbo et al., 1971), this technique had not been employed in probing the earth's atmosphere until the GPS/MET project (a-proof-of-concept occultation experiment), which utilized the GPS satellites for the earth's atmosphere studies. The GPS RO methods differ from most other satellite remote sensing methods in that they use measurements of phase rather than intensity. As the GPS signals are regulated by atomic clocks, the GPS occultation

tation measurements do not need additional calibration. These features make the GPS RO technique a new and precise sounding technique for the earth's atmosphere and it has the potential to improve weather analyses, to monitor climate change, and to provide ionospheric data at higher resolution and better accuracy. The earlier RO missions (GPS/MET, CHAMP, and SAC-C) refined the systems and techniques of GPS sounding that led to the stage set for COSMIC, the first operational GPS occultation constellation. COSMIC satellites were launched in low-earth orbits (800 km) jointly by the Taiwan Space Organization and the UCAR of the US in April 2006.

In general, an occultation occurs when one of GPS satellites (acting as transmitter) sets or rises behind the earth's atmosphere as seen by the low-earth-orbit (LEO) satellites (acting as receiver). In elaborative sense, the radio signal transmitted from a very stable source (GPS transmitter) to the LEO receiver follows a path through the atmosphere that curves distinctively in response to atmospheric gradients in refractive index. As the crux of radio occultation technique is to transform that curve (bending) angle of the radio path to the atmospheric refractive index (under a number of assumptions), the lower atmospheric temperature, humidity, and ionospheric electron density at the tangent point of the ray path piercing through the atmosphere can be estimated in accordance with the relation between the refractive index  $n$  and the following parameters:

$$n = 1 + \left( \frac{77.6p}{T} + \frac{3730e}{T^2} - \frac{5.6e}{T} \right) \times 10^{-6}, \quad (1)$$

where  $p$  is pressure (hPa),  $T$  is temperature (K), and  $e$  is water vapor pressure (hPa). In this study, we have downloaded wet temperature profiles (wetPrf) provided by RO technique performed on COSMIC satellites from <http://www.cosmic.ucar.edu>.

The earlier GPS RO techniques including GPS/MET and CHAMP often suffered with the inability to record and retrieve rising occultations and penetrate the lowest 2-km range in the tropical troposphere because of the usage of a traditional phase-locked loop (PLL) in their LEO satellite receivers. The close-loop (CL) tracking approach of PLL in LEO re-

ceiver utterly fails to lock on signals associated with high dynamics that often present in the atmospheric boundary layer (Ao et al., 2009) as the PLL adjusts the frequency of the reference signal on the basis of previous measurements, instead of taking care of the original signal. It is true that the CL approach works well when there is sufficient signal-to-noise (SNR) and the signal dynamics are not too high, which is often not the case, particularly in and around the atmospheric boundary layer. However, in order to study important atmospheric convective parameters, which are very sensitive to temperature and moisture profiles near the lower troposphere, the atmospheric profiles below 5 km would be necessary. Since the COSMIC satellites have been implemented with an open-loop (OL) tracking approach, wherein the reference signal is "guessed" based on knowledge of the orbits, receiver clock drift, and estimate of the atmospheric Doppler shift and delay, more than 90% of COSMIC soundings penetrate below 1 km (Ao et al., 2009).

## 2.2 The HHT method

We applied a Hilbert-Huang Transform (HHT; Huang et al., 1998; Wu et al., 2009) on retrieving the COSMIC temperature profiles between May 2006 and May 2010. The combination of the well-known Hilbert spectral analysis (HAS) and the recently developed empirical mode decomposition (EMD), a procedure with which any complicated database can be decomposed into infinite and often small number of intrinsic mode functions (IMFs), is designated as HHT. Since the decomposition in the HHT method is based on the local characteristics of the data, it is highly adaptive in nature and deals very well the nonlinear and non-stationary data. For a review on HHT and its applications to geophysical studies, please refer to Huang and Wu (2008).

## 3. Observational results

### 3.1 Comparisons between temperature profiles

We first validate the COSMIC RO retrieved temperature profiles with the nearby radiosonde measurements at two equatorial stations. Figure 1 depicts vertical profiles of temperature from radiosonde (thin

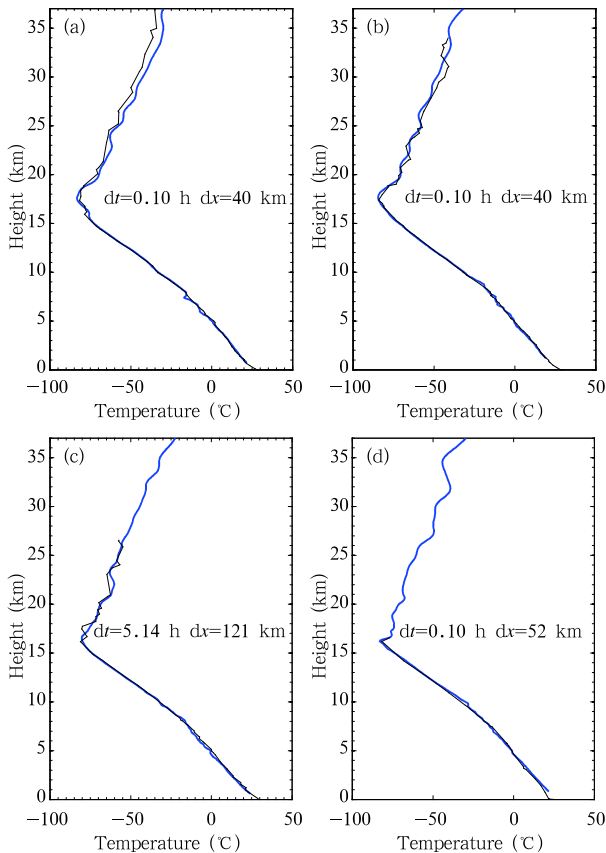


**Fig. 1.** Vertical profiles of temperature over Maldives ( $0.4^{\circ}\text{S}$ ,  $73^{\circ}\text{E}$ ) measured with radiosonde (thin lines) and nearby GPS retrievals (thick lines) on (a) 8 January 2007 and (b) 9 January 2007, and over Singapore ( $1^{\circ}\text{N}$ ,  $104^{\circ}\text{E}$ ) on (c) 18 October 2006 and (d) 1 January 2007.

line) and from nearby COSMIC GPS RO measurement (thick line) over Gan/Maldives ( $0.4^{\circ}\text{S}$ ,  $73^{\circ}\text{E}$ ) and over Singapore ( $1^{\circ}\text{S}$ ,  $104^{\circ}\text{E}$ ). Note that  $dt$  and  $dx$  in all panels indicate the differences in time and location between radiosonde and GPS RO measurements. It is evident from Fig. 1 that the temperature profiles from these two types of measurements show good consistency, thereby providing confidence in using COSMIC RO retrieved temperature in the studies of atmospheric dynamics.

Earlier studies conducted at different longitude sectors have also found a good agreement between GRP RO retrieved and radiosonde measured temperatures. For example, a validation study performed by Rao et al. (2009) at Gadanki ( $13.48^{\circ}\text{N}$ ,  $79.2^{\circ}\text{E}$ ), a tropical station in the Indian longitude zone, re-

vealed a mean difference of less than 1 K from 10 to 27 km between COSMIC and radiosonde temperatures. Kishore et al. (2009) performed a validation study using the operational stratospheric analyses including the NCEP reanalysis, the Japan 25-yr Reanalysis (JRA-25), and the United Kingdom Met Office (UKMO) datasets. Good agreement was observed between the COSMIC and the various reanalysis products, with the mean global difference and differences in the height range from 8 to 30 km all less than 1 K. Largest deviations were observed over polar latitudes and at the tropical tropopause with differences of 2–4 K. Collocated global atmospheric temperature profiles from radiosondes and COSMIC GPS RO satellites have been compared for April 2008–October 2009 by Sun et al. (2010). They found that in the troposphere, the temperature standard deviation errors were 0.35 K per 3 h and 0.42 K per 100 km. Comparative studies by Zhang et al. (2011) between GPS RO retrieved temperature profiles from both CHAMP and COSMIC satellites and those from 38 Australian radiosonde stations have shown a very good agreement between the two types of datasets. Specifically, Zhang et al. (2011) found the mean temperature difference between radiosonde and CHAMP to be  $0.39^{\circ}\text{C}$ , while it was  $0.37^{\circ}\text{C}$  between radiosonde and COSMIC satellites.

### 3.2 Kelvin waves and their identification

As most of the Kelvin waves are concentrated around the equator (Mote et al., 2002), we examine the COSMIC GPS RO retrieved temperature profiles within  $\pm 5^{\circ}$  latitudes from September 2006 to August 2009. By adopting the following procedure, we try to extract the Kelvin wave attributes in the temperature profiles. First, the temperature data are vertically interpolated onto a 500-m resolution. Note that the original COSMIC data are available at a 100-m vertical resolution and have an effective vertical resolution on the order of 500 m or above in the upper troposphere and lower stratosphere (UTLS). Due to the high inclination ( $72^{\circ}$ ) orbit of COSMIC satellites, the temperature profile data around the equator are rather sparse and hence a cubic interpolation in longitude is used to the temperature profile data to fill-in the miss-

ing data from 5- to 30-km altitudes (Fig. 2). Figure 2 shows the longitudinal temperature profile (stars) at 17 km on 2 September 2006 over the entire equatorial region ( $5^{\circ}\text{S}$ – $5^{\circ}\text{N}$ ) and the cubic interpolation data ( $T$ ) (solid line) as well as the 3rd order polynomial fit (dashed line). Second, we use a 3rd order polynomial ( $T_0$ ) regression to best fit to the interpolated data, which is considered to be background temperature variation. Note that the 3rd order polynomial fit has been applied to the time series at each individual height separately from 5 to 30 km. The background values are then removed from each temperature profile corresponding to each altitude and the resulting fluctuation ( $T' = T - T_0$ ) is utilized to identify the Kelvin wave features.

Furthermore, the fluctuation data during every three-month period are put together as ensembles to show the seasonal variation of Kelvin wave activity for the September equinox (SON: September, October, and November), December solstice (DJF: December, January, and February), March equinox (MAM: March, April, and May), and June solstice (JJA: June, July, and August) seasons of different years. Figure 3a shows interpolated data for fall 2006 between 5- and 30-km altitudes and Fig. 3b shows the cubic interpolation data during the same period for the entire globe at 17 km. It is clear from Fig. 3a that the tropopause is located at around 17 km with temperatures of about  $-75^{\circ}\text{C}$  ( $198^{\circ}\text{K}$ ) throughout the globe. Finally, we applied a Fast Fourier Transform (FFT) to the large-scale temperature fluctuation components, and then performed incoherent integration on the output of the FFT to identify the typical characteristics of Kelvin waves including wave number, wave period in days, phase speed, and vertical wavelength. A comparison between the observed characteristics of Kelvin waves and the theoretical results are presented in Table 1. It is clear from Table 1 that most observational values bear a close proximity to theoretical values, showing the ability of the present methodology that we adopted in this study.

To verify how temperature anomalies computed using the COSMIC retrieved temperatures respond to different phases of ENSO, we examine the temperature anomalies at different altitudes during warm and cold

phases of ENSO. Figure 4 depicts the longitude-time diagrams of temperature fluctuations at 15 and 16 km (Figs. 4a and 4b), 17 and 18 km (Figs. 4c and 4d), and 19 and 20 km (Figs. 4e and 4f) during September 2006 and February 2007, which coincide with a warm ENSO phase. The most evident feature is that negative temperature anomalies appear at 16, 17, and

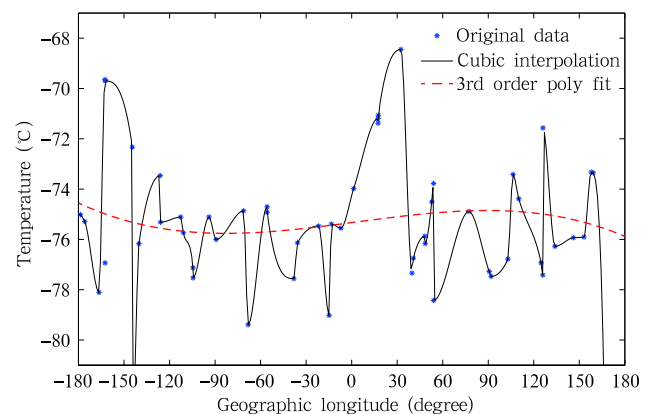


**Fig. 2.** Temperature data (stars) at 17 km on 2 September 2006 along with the cubic interpolation data (solid line) and the 3rd order polynomial fit (dashed line).

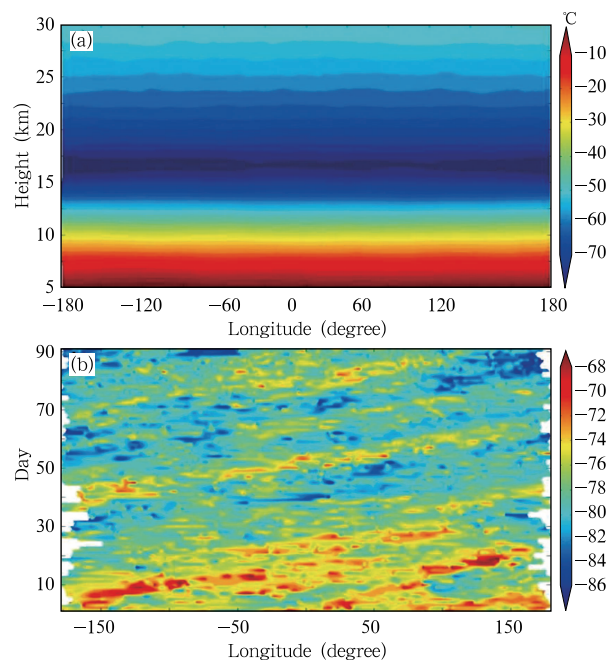


**Fig. 3.** (a) Global vertical temperature profiles during SON 2006 averaged between  $5^{\circ}\text{S}$  and  $5^{\circ}\text{N}$ , and (b) the cubic interpolated temperature data during SON 2006 averaged between  $5^{\circ}\text{S}$  and  $5^{\circ}\text{N}$ .

18 km, while positive values appear at 19 and 20 km, and the transition (from negative to positive) oc-

curs at the tropopause altitude, which agrees with the earlier research results (Scherllin-Pirscher et al., 2012).

**Table 1.** Wave properties such as wave number ( $s$ ), wave period ( $\tau$ ), phase speed ( $C_x$ ), and vertical wavelength ( $L_z$ ) during different seasons between 2006 and 2009 along with theoretical vertical wavelength ( $L_z$ ) in km

Season and year	Wavenumber ( $s$ )	Wave period in days ( $\tau$ )	Phase speed in $\text{km h}^{-1}$ ( $C_x$ )	Vertical wavelength in km ( $L_z$ )	Theoretical $L_z$ in km
September equinox/2006	1	15	75.6	5–6	5.02
December solstice/2006	1	17	92.6	6–8	5.45
March equinox/2007	2	10	83.3	5–8	4.8
June solstice/2007	1	17	87.5	6–12	7.3
September equinox/2007	2	9.5	77.5	6–10	9.2
December solstice/2007	1	15	86.8	6–7	12.0
March equinox/2008	2	12	77.2	9	7.9
June solstice/2008	1	13	76.8	8–9	9.9
September equinox/2008	1	14	85.2	6–7	8.5
December solstice/2008	2	9	70.2	10	8.6
March equinox/2009	2	11	88.2	11	9.2
June solstice/2009	1	12	81.6	8	9.8

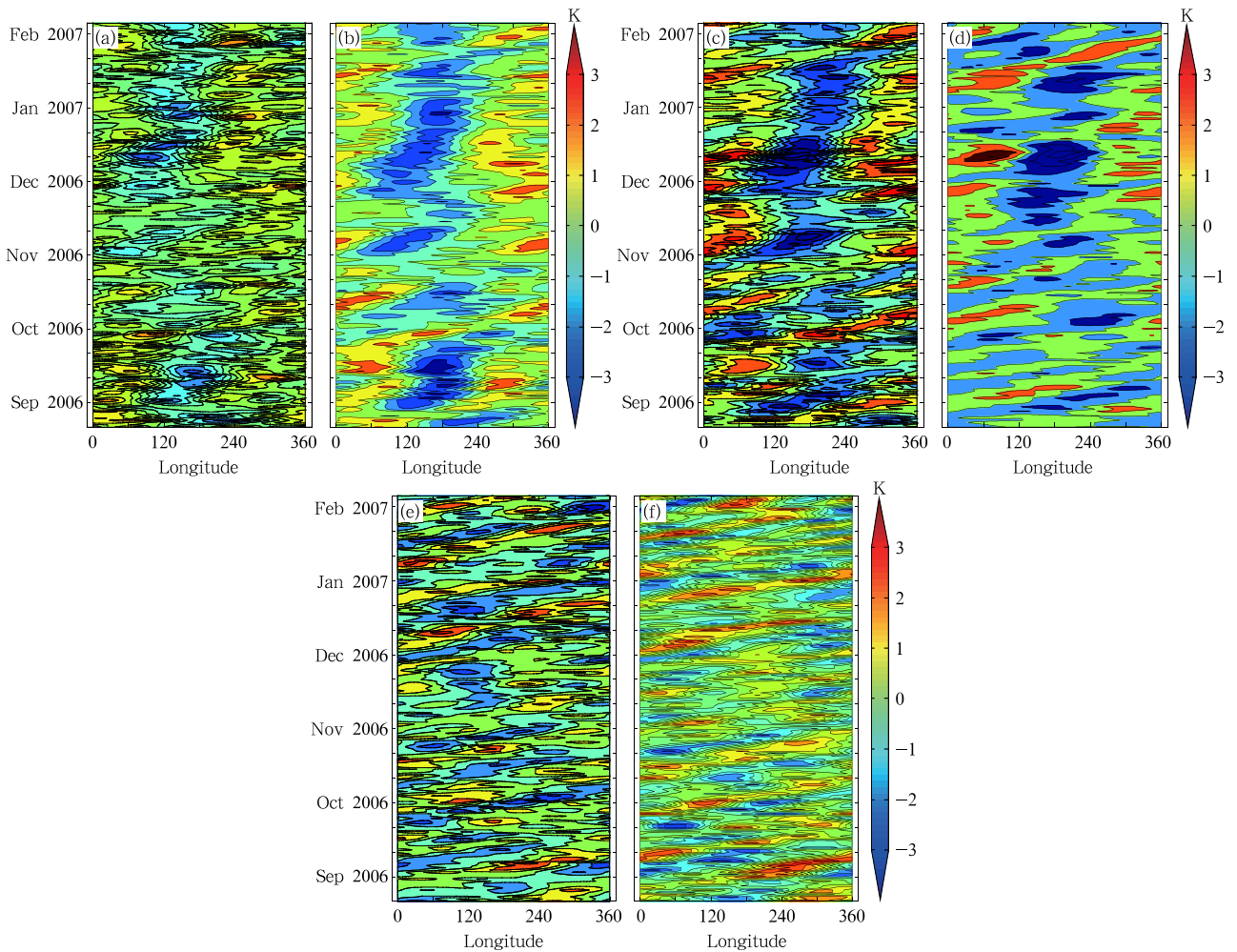


**Fig. 4.** Longitude-time evolution of temperature fluctuations over  $5^{\circ}\text{S}$ – $5^{\circ}\text{N}$  during September 2006 and February 2007 at altitudes of (a) 15, (b) 16, (c) 17, (d) 18, (e) 19, and (f) 20 km.

Figure 5 depicts the longitude-time diagrams of temperature fluctuations from March to August 2007, which coincides with a cool ENSO phase. Though the temperature anomalies at 15, 16, 17, and 18 km exhibit negative values during the El Niño phase (Figs. 4a–d), the anomaly trends at 19 and 20 km are not associated with higher positive values as observed during the El Niño phase (see Figs. 4e–f). The above results are consistent with the findings of Yang and Hoskins (2013), who studied the impact of ENSO on atmospheric Kelvin waves.

It is also clear that the temperature fluctuations from November 2006 to February 2007 at altitudes of 16, 17, and 18 km are characterized by the known climatological structure of cold temperatures over 90°E–160°W and maximum convection over In-

donesia (Highwood and Hoskins, 1998; Seidel et al., 2001; Randel et al., 2003; Randel and Wu, 2005). The temperature minimum in the cold region varies episodically during these months (in response to variations in deep convection), but the overall patterns are quasi-stationary. In contrast, temperature fluctuations at altitudes of 19 and 20 km show a zonal wavenumber-1 structure with regular eastward propagation. These results are consistent with previous reports such as Garcia and Salby (1987) and Randel and Wu (2005). Using CHAMP and SAC-C RO data, Randel and Wu (2005) found the quasi-stationary wave structures near the tropopause (17 km) for 6 consecutive months starting from October 2001 to March 2002 (Fig. 4a of their paper) and regular eastward propagating waves at height of 19 km (Fig. 4b of their paper).

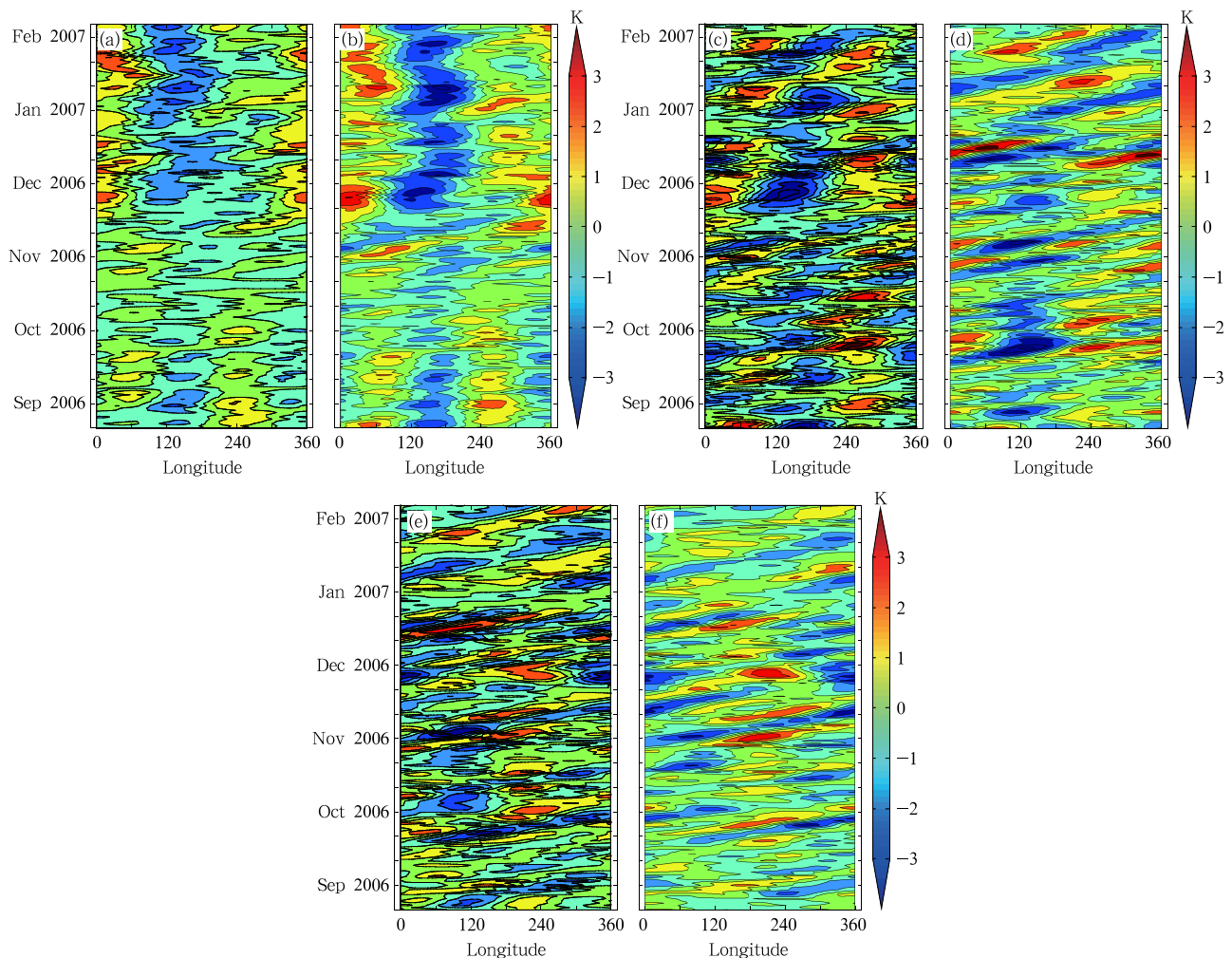


**Fig. 5.** As in Fig. 4, but during March–August 2007.

Identification of the characteristic temporal and spatial scales of zonally propagating planetary waves in deep tropical convection has been carried out by applying spectral analysis to satellite-observed outgoing longwave radiation (OLR) (Wheeler and Kiladis, 1999; Randel and Wu, 2005, and others). It is well known that deep convection is a primary source of wave variability in the tropical atmosphere (Salby and Garcia, 1987; Wheeler and Kiladis, 1999) and it is of great importance to study the relationship between the large-scale Kelvin waves observed in GPS data and the deep convection during the same time period. Since OLR can be considered as a proxy for deep convection, we analyze the OLR data to understand the relation between Kelvin waves and deep convective activity. Figure 6 shows a longitude-time diagram of the OLR data averaged over  $5^{\circ}\text{N}$ – $5^{\circ}\text{S}$  from January 2006 to January 2013. It is obvious that three longitude sectors including  $10^{\circ}$ – $30^{\circ}\text{E}$ ,  $60^{\circ}$ – $170^{\circ}\text{E}$ , and  $280^{\circ}$ – $310^{\circ}\text{E}$  are characterized by relatively low OLR values (often  $< 180 \text{ W m}^{-2}$ ), particularly over  $60^{\circ}$ – $170^{\circ}\text{E}$ , compared to the rest of the globe. Significantly associated convective activities are observed during boreal winter months, with eastward propagating features. As cold temperatures also present around the  $80^{\circ}$ – $190^{\circ}\text{E}$  longitude sector at altitudes of 16, 17, and 18 km (Figs. 4b–d and Figs. 5a–d), it is inferred that these cold temperatures are excited by those deep convective activities. Therefore, the tropical convection generated over the Indonesian region during the present observation period may be the plausible source for Kelvin waves (Salby and Garcia, 1987; Wheeler and Kiladis, 1999). Nevertheless, it is shown that the phase speed of the propagating OLR patterns is much slower than the Kelvin waves observed in the present study, so the Kelvin waves are not continuously coupled to convection. It is very likely that the observed Kelvin waves are more consistent with free modes forced by the broad spectrum of convective variability, especially that over the convection-active Indonesian region (Randel and Wu, 2005; Ratnam et al., 2006).

Evolution of the monthly-mean zonal (east-west) winds at 16.5–28-km altitude are presented in Fig. 7 for the period of January 2006–October 2010. The

stratospheric QBO is dominant for two complete cycles, with downward propagation particularly from 17 km and with dominant amplitudes between 23 and 28 km. The thick black double arrow in Fig. 7 indicates the time period (September 2006 to August 2009) during which the characteristics of Kelvin waves are studied. Note that the time period of the present study includes almost two complete cycles of QBO with eastward phases starting from March 2006 to May 2007 and from August 2008 to April 2009, and westward phases from June 2007 to July 2008 and from May 2009 to July 2010.

In order to examine the Kelvin wave activity in both phases of QBO, vertical temperature fluctuation

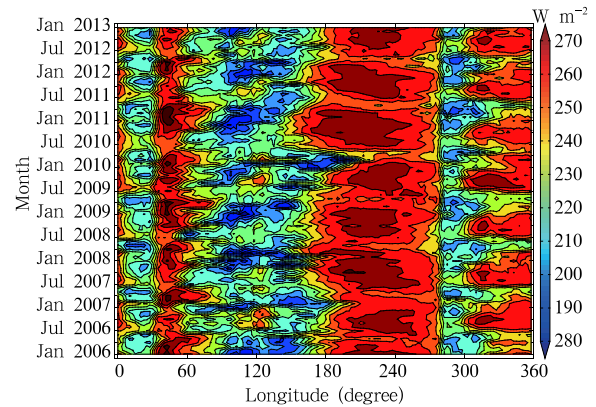


**Fig. 6.** OLR averaged over  $5^{\circ}\text{S}$ – $5^{\circ}\text{N}$  from January 2006 to January 2013.

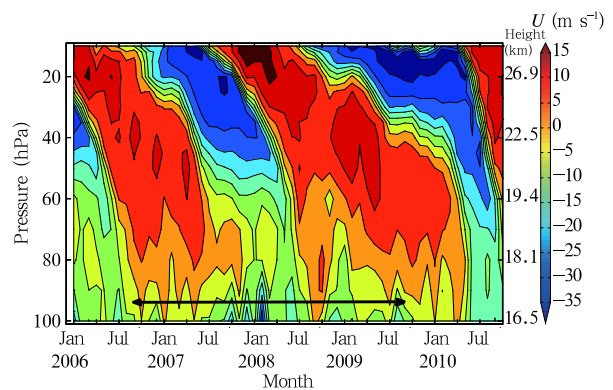


**Fig. 7.** Time-height diagram of zonal winds derived from radiosonde observations over Singapore between January 2006 and October 2010, showing QBO features at stratospheric altitudes. The thick black double arrow indicates the duration during which Kelvin waves are present.

components are selected and presented in Fig. 8 for 4 days: (1) 13/14 October 2006 (Fig. 8a; eastward phase), (2) 15/16 May 2007 (Fig. 8b; eastward phase), (3) 27/28 August 2007 (Fig. 8c; westward phase), and (4) 19/20 February 2008 (Fig. 8d; westward phase), respectively. It is obvious that the eastward phase tilt with height (characteristic of Kelvin waves) is evident in all panels with a coherent vertical structure over 11–27 km and the largest amplitudes near and above the tropical tropopause. Vertical wavelengths in Figs. 8a and 8b are 10 and 12 km, while the phase lines of temperature waves in Figs. 8c and 8d are extending into the upper troposphere with more upright behavior and with longer vertical wavelengths around 13 and 14 km. Further, the Kelvin wave event in Fig. 8d is relatively stronger than other Kelvin wave events. The associated relation between Kelvin waves and background winds is most probably due to thermal damping pro-

posed earlier (Shiotani and Horinouchi, 1993). A similar analysis is performed from 10 to 30 km for the entire time series between September 2006 and September 2008 and Fig. 9 depicts time-height variations of the amplitudes of wavenumbers 1 and 2 (averaged). It is obvious that an increased (decreased) tendency in wave amplitudes is seen particularly above 18 km during westward (eastward) phase of QBO, i.e., between September 2007 and September 2008 (September 2006 and August 2007). It has been reported that Kelvin waves generally do not exist above 20-km altitude, except during a strong westward phase of QBO or during a strong eastward shear (Ratnam et al., 2006). Our observational results agree with the findings of Ratnam et al. (2006), who discussed how Kelvin wave activity with enhanced features near the tropopause could enhance the tropical tropopause height. Similarly, it is also found in this study that the amplitudes of Kelvin

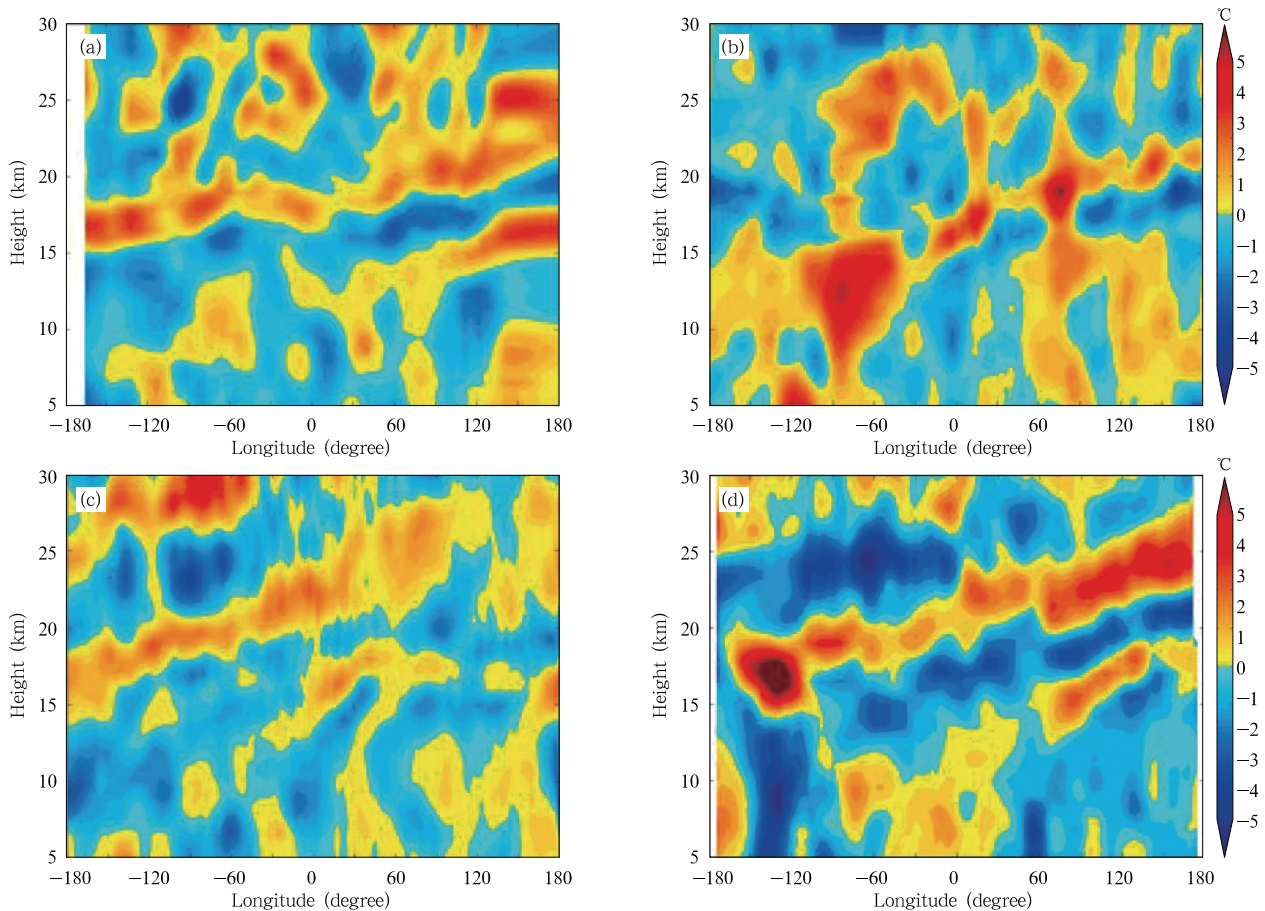


**Fig. 8.** Kelvin waves in temperature fluctuations during (a, b) eastward phase and (c, d) westward phase of QBO.

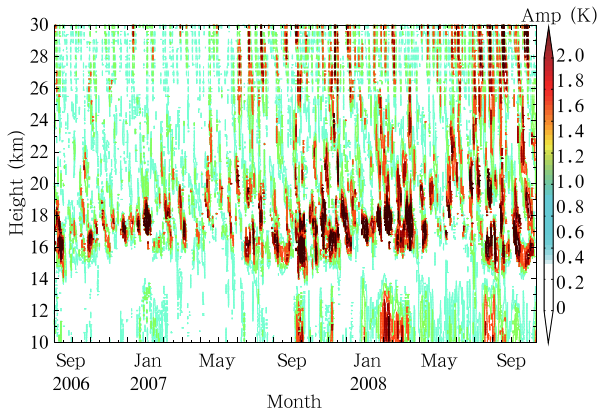


**Fig. 9.** Time-height variations of Kelvin wave amplitudes observed at equatorial latitudes ( $\pm 10^\circ$ ) from the COSMIC GPS RO satellites between September 2006 and September 2008.

waves increase the most near the altitude of tropopause irrespective of the phase of QBO (Fig. 9).

### 3.3 ENSO and QBO signatures in temperature profiles

Before analyzing ENSO features observed in COSMIC temperatures, we have initially used the multivariate ENSO index (MEI) (Randel et al., 2009) in order to know exactly the temporal variations of ENSO features during the study period (2005–2011). The MEI (available at <http://www.esrl.noaa.gov/psd/enso/mei/mei.html>) is a Pacific-basin-wide index created from several atmospheric and oceanic variables such as the sea surface temperature, OLR, and the pressure gradient between two remote locations across the Pacific, with atmospheric variables lagged by about two months (Randel et al., 2009). Figure 10 depicts the time series of MEI between January 2005 and January 2012, wherein the positive (negative) values represent a warm (cold) El Niño (La Niña) event. The horizontal dashed lines represent the  $\pm 1\sigma$  standard deviation, indicating the strength of warm or cold ENSO events. It is clear from Fig. 10 that the warm ENSO (El Niño) occurs around August–December 2006 and November–March 2010, while the cold ENSO (La Niña) occurs between January and May 2008 and again between July 2010 and June 2011, respectively.

Before applying the powerful HHT, we removed

the annual mean in the temperature data to obtain the temperature anomalies. Then, we applied the multi-dimensional ensemble empirical mode decomposition (MEED; Wu et al., 2009), a decomposition method used for multi-dimensional data, on temperature anomalies. Though the resultant IMFs show irregular patterns, the fifth IMF (C5) clearly shows the presence of ENSO and QBO features in the temperature anomalies. It is seen in Fig. 11a that the HHT-MEED decomposed IMF C5 component exhibits an ENSO cold phase (La Niña) around March 2008 from western Pacific ( $\sim 100^\circ\text{E}$ ) to eastern Pacific ( $150^\circ\text{W}$ ), consistent with the MEI in Fig. 10. On the other hand, a weak warm phase of ENSO (El Niña) is observed between August 2006 and January 2007 from the Indonesian sector ( $\sim 80^\circ\text{E}$ ) to western Pacific ( $160^\circ\text{E}$ ), whereas a strong El Niña appears around February 2010 from  $80^\circ$  to  $180^\circ\text{E}$  in accordance with the MEI in Fig. 10. Due to strong confounding effects of QBO (Scherllin-Pirscher et al., 2012), the ENSO features in the COSMIC retrieved temperature anomalies could not be revealed above the 16-km altitude. Figure 11b shows the HHT-MEED decomposed IMF C5 component at 24-km height, wherein the QBO features are clearly demonstrated. For instance, the easterly phase of QBO is found between February and November 2006, and again, between December 2007 and September 2008; whereas the westerly phase of

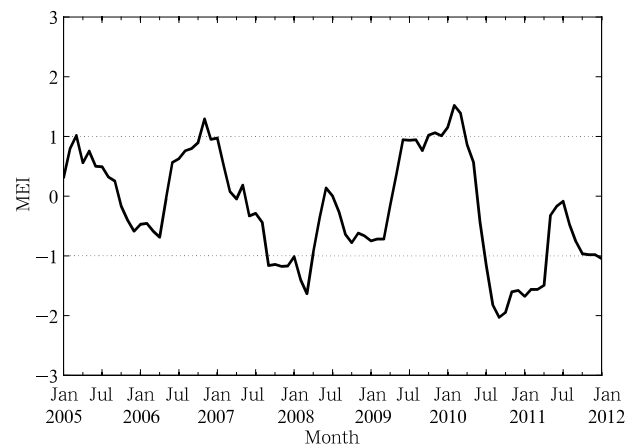


**Fig. 10.** Time series of MEI from January 2005 to January 2012. The horizontal dashed lines represent the  $\pm 1\sigma$  standard deviation.

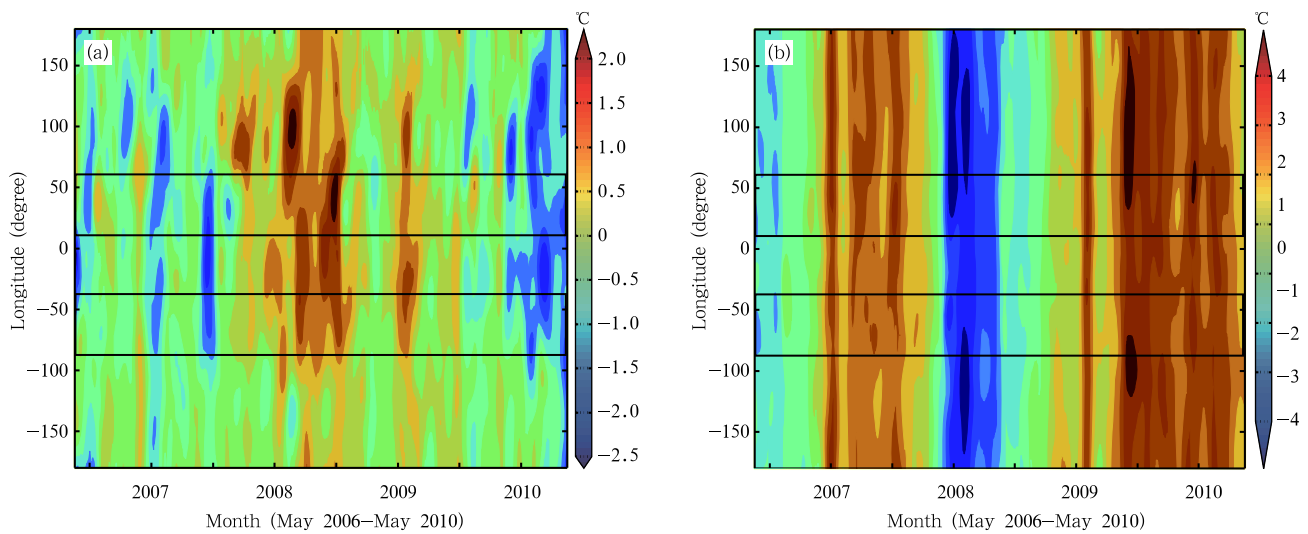


**Fig. 11.** HHT-MEED decomposed C5 components of temperature anomalies showing (a) ENSO at 15 km and (b) QBO at 24 km during 2006–2010.

QBO is found between December 2006 and November 2007 as well as October 2008 and March 2010. These QBO features not only reflect the QBO signature in zonal winds over Singapore ( $1^{\circ}\text{N}$ ,  $100^{\circ}\text{E}$ ) as presented earlier in this paper, but also show a one-to-one correspondence with the results presented by other researchers (Steiner et al., 2011).

#### 4. Conclusions

With the recent GPS RO technique performed on six COSMIC micro-satellites, it has become possible for us to understand the atmospheric planetary-scale equatorially trapped waves and other large-scale wave structures including ENSO and QBO in temperature profiles. The promising results of the present study encourage us to apply the analysis procedures used in this study to datasets to be provided by ensuing RO techniques including COSMIC-2 that is going to be launched during the mid 2016, with which more details can be revealed as COSMIC-2 will be capable of producing 4–5 times higher volume of data compared to COSMIC, particularly over tropical regions as the inclination of the six COSMIC-2 satellites is only  $24^{\circ}$  (Mannucci et al., 2012).

The results of the present study are summarized

as follows. 1) A preliminary comparison between COSMIC retrieved and radiosonde measured temperature profiles reveals a one-to-one correspondence between them, indicating the applicability of the GPS RO retrieved profiles. 2) The Kelvin waves derived from the temperature files show zonal wavenumbers of either 1 or 2, with eastward phase propagation in longitude-time section and at periodicities of greater than 10 days (slow Kelvin waves). 3) The Kelvin waves show decreasing tendencies during the eastward phase of QBO, but increasing tendencies during the westward phase of QBO. 4) The OLR data confirm the presence of deep convection around the  $60^{\circ}$ – $180^{\circ}\text{E}$  longitude sectors, which could have acted as a source for the observed Kelvin waves. 5) With the help of recently developed HHT-MEED decomposition, ENSO and QBO signatures have been clearly identified in the COSMIC retrieved temperature anomalies. The ENSO and the QBO features are most significant at around 1–15-km altitude and between 16 and 30 km. These results are consistent with previous observational results. 6) The temperature anomalies computed using the COSMIC retrieved temperatures during different phases of ENSO are critically evaluated. Higher (lower) positive values occur during the warm (cool) phase of ENSO above the tropical tropopause height.

**Acknowledgments.** The COSMIC temperature data were obtained from the COSMIC Data Analysis and Archive Centre (CDAAC). OLR data were provided by NOAA (<http://www.cdc.noaa.gov>). Dr. G. Uma is grateful to the Department of Science and Technology (DST), Government of India for offering her a Women Scientist Fellowship (WOS-A-SR/WOS-A/PS-01/2011).

## REFERENCES

- Alexander, M. J., and J. R. Holton, 1997: A model study of zonal forcing in the equatorial stratosphere by convectively induced gravity waves. *J. Atmos. Sci.*, **54**, 408–419.
- Alexander, S. P., T. Tsuda, Y. Kawatani, et al., 2008: Global distribution of atmospheric waves in the equatorial upper troposphere and lower stratosphere: COSMIC observations of wave mean flow interactions. *J. Geophys. Res.*, **113**, D24115.
- Angell, J. K., and J. Korshover, 1964: Quasi-biennial variations in temperature, total ozone, and tropopause height. *J. Atmos. Sci.*, **21**, 479–492.
- Anthes, R. A., D. Ector, D. C. Hunt, et al., 2008: The COSMIC/FORMOSAT-3 mission: Early results. *Bull. Amer. Meteor. Soc.*, **89**, 313–333.
- , 2011: Exploring earth’s atmosphere with radio occultation: Contributions to weather, climate, and space weather. *Atmos. Meas. Tech.*, **4**, 1077–1103.
- Ao, C. O., G. A. Hajj, T. K. Meehan, et al., 2009: Rising and setting GPS occultations by use of open-loop tracking. *J. Geophys. Res.*, **114**, D04101, doi: 10.1029/2008JD010483.
- Baldwin, M. P., L. J. Gray, T. J. Dunkerton, et al., 2001: The quasi-biennial oscillation. *Rev. Geophys.*, **39**, 179–229.
- Brahmanandam, P. S., Y. H. Chu, and J. Liu, 2010: Observations of equatorial Kelvin wave modes in FORMOSAT-3/COSMIC GPS RO temperature profiles. *Terr. Atmos. Ocean. Sci.*, **21**(5), 829–840.
- , Y. H. Chu, K.-H. Wu, et al., 2011: Vertical and longitudinal electron density structures of equatorial E- and F-regions. *Ann. Geophys.*, **29**, 81–89.
- , U. Gouthu, J. Y. Liu, et al., 2012: Global S4 index variations observed using FORMOSAT-3/COSMIC GPS RO technique during a solar minimum year. *J. Geophys. Res.*, **117**, A09322, doi: 10.1029/2012JA017966.
- Canziani, P. O., J. R. Holton, E. F. Fishbein, et al., 1994: Equatorial Kelvin waves: A UARS MLS view. *J. Atmos. Sci.*, **51**, 3053–3076.
- , and J. R. Holton, 1998: Kelvin waves and the quasi-biennial oscillation: An observational analysis. *J. Geophys. Res.*, **103**, 31509–31521.
- Chu, Y.-H., P. S. Brahmanandam, C.-Y. Wang, et al., 2011: Coordinated sporadic E-layer observations made with Chung-Li 30 MHz radar, ionosonde and FORMOSAT-3/COSMIC satellites. *J. Atmos. Terr. Phys.*, **73**, 883–894.
- Dunkerton, T. J., 1997: The role of gravity waves in the quasi-biennial oscillation. *J. Geophys. Res.*, **102**, 26053–26076.
- Ern, M., P. Preusse, M. Krebsbach, et al., 2008: Equatorial wave analysis from SABER and ECMWF temperatures. *Atmos. Chem. Phys.*, **8**, 845–869.
- Evan, S., M. J. Alexander, and J. Dudhia, 2012: WRF simulations of convectively-generated gravity waves in opposite QBO phases. *J. Geophys. Res.*, **117**, 1–17.
- Fjeldbo, G., A. J. Kliore, and V. R. Eshleman, 1971: The neutral atmosphere of Venus as studied with the Mariner V radio occultation experiments. *The Astronomical Journal*, **76**, 123–140.
- Fujiwara, M., K. Kita, and T. Ogawa, 1998: Stratosphere-troposphere exchange of ozone associated with the equatorial Kelvin wave as observed with ozonesondes and rawinsondes. *J. Geophys. Res.*, **103**, 19173–19182.
- , F. Hasebe, M. Shiotani, et al., 2001: Water vapor control at the tropopause by equatorial Kelvin waves observed over the Galápagos. *Geophys. Res. Lett.*, **28**, 3143–3146.
- , S.-P. Xie, M. Shiotani, et al., 2003: Upper-tropospheric inversion and easterly jet in the tropics. *J. Geophys. Res.*, **108**, 4796, doi: 10.1029/2003JD003928.
- Garcia, R. R., and M. L. Salby, 1987: Transient response to localized episodic heating in the tropics. Part II: Far-field behavior. *J. Atmos. Sci.*, **44**, 499–532.
- Hajj, G. A., C. O. Ao, B. A. Iijima, et al., 2004: CHAMP and SAC-C atmospheric occultation results and intercomparisons. *J. Geophys. Res.*, **109**, doi: 10.1029/2003JD003909.
- Highwood, E. J., and B. J. Hoskins, 1998: The tropical tropopause. *Quart. J. Roy. Meteor. Soc.*, **124**, 1579–1604.

- Hitchman, M. H., and C. B. Leovy, 1988: Estimation of the Kelvin wave contribution to the semiannual oscillation. *J. Atmos. Sci.*, **45**, 1462–1475.
- Holton, James R., and R. S. Lindzen, 1972: An updated theory for the quasi-biennial cycle of the tropical stratosphere. *J. Atmos. Sci.*, **29**, 1076–1080.
- Huang, N. E., Z. Shen, S. R. Long, et al., 1998: The empirical mode decomposition and the Hilbert spectrum for nonlinear and non-stationary time series analysis. *Proc. R. Soc. Lond. A*, **454**, 903–993, doi: 10.1098/rspa.1998.0193.
- , and Z. H. Wu, 2008: A review on Hilbert-Huang Transform: Method and its applications to geophysical studies. *Rev. Geophys.*, **46**, RG2006, doi: 10.1029/2007RG000228.
- Kawatani, Y., S. Watanabe, K. Sato, et al., 2010: The roles of equatorial trapped waves and internal inertia-gravity waves in driving the quasi-biennial oscillation. Part I: Zonal mean wave forcing. *J. Atmos. Sci.*, **67**(4), 963–980.
- Kishore, P., S. P. Namboothiri, J. H. Jiang, et al., 2009: Global temperature estimates in the troposphere and stratosphere: A validation study of COSMIC/FORMOSAT-3 measurements. *Atmos. Chem. Phys.*, **9**, 897–908.
- Lindzen, R. S., 2003: The interaction of waves and convection in the tropics. *J. Atmos. Sci.*, **60**, 3009–3020.
- Mannucci, A. J., S. T. Lowe, C. O. Ao, et al., 2012: New science opportunities on COSMIC-2/FORMOSAT-7. Sixth COSMIC/FORMOSAT-3 Data User's Workshop, Boulder, Colorado, USA.
- Melbourne, W. G., E. S. Davis, G. A. Hajj, et al., 1994: *The Application of Spaceborne GPS to Atmospheric Limb Sounding and Global Change Monitoring*. JPL Publication, 147 pp.
- Mote, P. W., T. J. Dunkerton, and D. Wu, 2002: Kelvin waves in stratospheric temperature observed by the Microwave Limb Sounder. *J. Geophys. Res.*, **107**(D14), 4218.
- Pires, P., J.-L. Redelsperger, and J.-P. Lafore, 1997: Equatorial atmospheric waves and their association to convection. *Mon. Wea. Rev.*, **125**, 1167–1184.
- Potula, B. S., Y.-H. Chu, G. Uma, et al., 2011: A global comparative study on the ionospheric measurements between COSMIC radio occultation technique and IRI model. *J. Geophys. Res.*, **116**, A02310, doi: 10.1029/2010JA015814.
- Randel, W. J., F. Wu, and W. Rivera Ríos, 2003: Thermal variability of the tropical tropopause region derived from GPS/MET observations. *J. Geophys. Res.*, **108**(D1), 4024, doi: 10.1029/2002JD002595.
- , and —, 2005: Kelvin wave variability near the equatorial tropopause observed in GPS radio occultation measurements. *J. Geophys. Res.*, **110**, doi: 10.1029/2004JD005006.
- , K. P. Shine, J. Austin, et al., 2009: An update of observed stratospheric temperature trends. *J. Geophys. Res.*, **114**, D02107, doi: 10.1029/2008JD010421.
- Rao, D. N., M. Venkat Ratnam, S. K. Mehta, et al., 2009: Validation of the COSMIC radio occultation data over Gadanki (13.48°N, 79.2°E): A tropical region. *Terr. Atmos. Ocean. Sci.*, **20**, 59–70.
- Ratnam, M. V., T. Tsuda, T. Kozu, et al., 2006: Long-term behavior of the Kelvin waves revealed by CHAMP/GPS RO measurements and their effects on the tropopause structure. *Ann. Geophys.*, **24**, 1355–1366.
- Salby, M. L., D. L. Hartmann, P. L. Bailey, et al., 1984: Evidence for equatorial Kelvin modes in Nimbus-7 LIMS. *J. Atmos. Sci.*, **41**, 220–235.
- , and R. R. Garcia, 1987: Transient response to localized episodic heating in the tropics. Part I: Excitation and short-time near-field behavior. *J. Atmos. Sci.*, **44**, 458–498.
- Sasi, M. N., and V. Deepa, 2001: Seasonal variation of equatorial wave momentum fluxes at Gadanki (13.5°N, 79.2°E). *Ann. Geophys.*, **19**, 985–990, doi: 10.5194/angeo-19-985-2001.
- Scherllin-Pirscher, B., C. Deser, S.-P. Ho, et al., 2012: The vertical and spatial structure of ENSO in the upper troposphere and lower stratosphere from GPS radio occultation measurements. *Geophys. Res. Lett.*, **39**, L20801, doi: 10.1029/2012GL053071.
- Seidel, D. J., R. J. Ross, J. K. Angell, et al., 2001: Climatological characteristics of the tropical tropopause as revealed by radiosondes. *J. Geophys. Res.*, **106**, 7857–7878.
- Shiotani, M., and T. Horinouchi, 1993: Kelvin wave activity and the quasi-biennial oscillation in the equatorial lower stratosphere. *J. Meteor. Soc. Japan.*, **71**, 175–182.
- , J. C. Gille, and A. E. Roche, 1997: Kelvin waves in the equatorial lower stratosphere as revealed by cryogenic limb array etalon spectrometer temperature data. *J. Geophys. Res.*, **102**, 26131–26140.

- Smith, A. K., P. Preusse, and J. Oberheide, 2002: Middle atmosphere Kelvin waves observed in Cryogenic infrared Spectrometers and Telescopes for the Atmosphere (CRISTA) 1 and 2 temperature and trace species. *J. Geophys. Res.*, **107**, doi: 10.1029/2001JD000577.
- Sridharan, S., T. Tsuda, T. Nakamura, et al., 2006: Observations of the 7-day Kelvin wave in the tropical atmosphere during the CPEA campaign. *J. Meteor. Soc. Japan*, **84a**, 259–275.
- Steiner, A. K., B. C. Lackner, F. Ladstädter, et al., 2011: GPS radio occultation for climate monitoring and change detection. *Radio Sci.*, **46**, RS0D24, doi: 10.1029/2010RS004614.
- Sun, B. M., A. Reale, D. J. Seidel, et al., 2010: Comparing radiosonde and COSMIC atmospheric profile data to quantify differences among radiosonde types and the effects of imperfect collocation on comparison statistics. *J. Geophys. Res.*, **115**, D23104.
- Tindall, J. C., J. Thurnburn, and E. J. Highwood, 2006a: Equatorial waves in the lower stratosphere. Part I: A novel detection method. *Quart. J. Roy. Meteor. Soc.*, **132**, 177–194.
- , —, —, 2006b: Equatorial waves in the lower stratosphere. Part II: Annual and interannual variability. *Quart. J. Roy. Meteor. Soc.*, **132**, 195–212.
- Tsuda, T., Y. Murayama, H. Wiryo Sumarto, et al., 1994: Radiosonde observations of equatorial atmosphere dynamics over Indonesia: 1. Equatorial waves and diurnal tides. *J. Geophys. Res.*, **99**, 10491–10505.
- Uma, G., J. Y. Liu, S. P. Chen, et al., 2012: A comparison of the equatorial spread F derived by the international reference ionosphere and the S4 index observed by FORMOSAT-3/COSMIC during the solar minimum period of 2007–2009. *Earth Planets Space*, **64**, 467–471.
- Wallace, J. M., and V. E. Kousky, 1968: Observational evidence of Kelvin waves in the tropical stratosphere. *J. Atmos. Sci.*, **25**, 900–907.
- Wheeler, M., and G. N. Kiladis, 1999: Convectively coupled equatorial waves: Analysis of clouds and temperature in the wavenumber-frequency domain. *J. Atmos. Sci.*, **56**, 374–399.
- Wickert, J., C. Reigber, G. Beyerle, et al., 2001: Atmosphere sounding by GPS radio occultation: First results from CHAMP. *Geophys. Res. Lett.*, **28**(17), 3263–3266.
- Wu, Z., N. Huang, and Y. Chen, 2009: The multi-dimensional ensemble empirical mode decomposition method. *Advances in Adaptive Data Analysis*, **1**, 339–372.
- Yang, G. Y., and B. Hoskins, 2013: ENSO impact on Kelvin waves and associated tropical convection. *J. Atmos. Sci.*, doi: 10.1175/JAS-D-13-081.1.
- Zhang, K., E. Fu, D. Silcock, et al., 2011: An investigation of atmospheric temperature profiles in the Australian region using collocated GPS radio occultation and radiosonde data. *Atmos. Meas. Tech.*, **4**, 2087–2092.
- Zeng, Z., S.-P. Ho, S. Sokolovskiy, et al., 2012: Structural evolution of the Madden-Julian Oscillation from COSMIC radio occultation data. *J. Geophys. Res.*, **117**, D22108.